Liquid Column Separation Due to Fluid Hammer Occurrence in Propellant Lines

Marcos Lema,* Anne Gosset,† and Fernando López Peña‡
University of A Coruña, 15001 A Coruña, Spain
and
Johan Steelant§
ESA, 2200 AG Noordwijk ZH, The Netherlands

https://doi.org/10.2514/1.B38451

When a pressurized liquid enters a pipeline with a closed end and under vacuum conditions, the resulting liquid front suddenly is brought to rest at the end of the pipe. This type of flow configuration is found in propulsion systems of satellites during priming operation and induces a fluid hammer followed by a column separation, generating a multiphase gas/vapor bubble. This paper aims at explaining the column separation mechanism by solving the momentum equation for the liquid column moving in the pipeline when column separation occurs and by applying the integral form of the conservation principles to expansion and compression waves within the flow. The resulting model provides the velocity and position of the liquid front during column separation. Thus, the size and duration of the multiphase bubble can be determined, and the variables involved in the process are identified, which helps the analysis of applications where this complex phenomenon is involved. It is shown that the initial velocity of the liquid front during column separation is the main parameter, which itself is a function of the fuel tank pressure and the fluid hammer pressure rise. The comparison of the predictions with experimental data shows an excellent agreement.

Nomenclature

A = surface area, m^2
a = speed of sound, $m \cdot s^{-1}$
B = empirical function, bar
C = empirical function
D = pipe diameter, m
e = pipe wall thickness, m
f_m = body force, N
I = unit tensor
L = pipe length, m
M = molecular weight, $g \cdot mol^{-1}$
m = fluid mass, kg
n = normal vector
P = pressure, Pa
S = control surface, m^2
s = surface, m^2
T = temperature, °C
t = time, s
U = cross-sectional average liquid front velocity, $m \cdot s^{-1}$
u = velocity vector, $m \cdot s^{-1}$
V = fluid volume and control volume, m^3
x = spatial coordinate, m
y = spatial coordinate, m
α = void fraction
γ = adiabatic index
ϵ = pipe roughness, m
λ = friction factor
ρ = density, $kg \cdot m^{-3}$
τ = shear stress, Pa

Subscripts

b = behind (for example, fluid velocity behind the compression or expansion wave)
c = control surface (for example, control surface velocity)
f = front (for example, fluid velocity in front of the shock compression or expansion wave)
m = mass or body (for example, body force)
p = vacuum conditions in the test element
T = tank (for example, tank pressure)
v = vapor (for example, vapor pressure)
w = wall
wh = water hammer (for example, water hammer of fluid hammer pressure peak)
0 = initial condition

Received 10 March 2021; revision received 18 July 2022; accepted for publication 28 August 2022; published online 30 September 2022.

*Associate Professor, Center for Information and Communications Technology Research, Maestranza 9; marcos.lema@udc.es.
†Associate Professor, Center for Technological Research, Maestranza 9; anne.gosset@udc.es.
‡Professor, Center for Information and Communications Technology Research, European Space Research and Technology Centre, Keplerlaan 1; fernando.lopez.pena@udc.es.
§Senior Project Engineer, Flight Vehicles and Aerothermodynamics Engineering Section (TEC-MPA), Maestranza 9; Johan.Steelant@esa.int.

I. Introduction

FILLING a piping system can cause a fluid hammer to occur in those cases where the flow is forced to stop. This scenario is particularly hazardous when a liquid fills a pipeline that is under vacuum conditions by opening a fast valve, which causes a high flow acceleration before stopping at the closed end, inducing a fluid hammer pressure rise. This flow configuration is commonly found in propulsion systems of satellites during priming operation, where the propellant lines initially kept under vacuum conditions are filled with pressurized liquid propellant by opening a one-time use pyrotechnic valve, as described in Refs. [1,2].

The first studies on fluid hammers focused on pipelines filled with water experiencing flow pressure transients. However, the fluid hammer not only leads to high-pressure peaks in the fluid but also to regions with low static pressure, such as downstream of a fast-closing valve [3–5], due to the arrival of a reflected expansion wave after fluid hammer occurrence [6,7] or at knee points of the piping system [8]. These low pressures can reach values that are well below the vapor pressure, thus leading to cavitation. According to the review by Bergant et al. [9] and the work of Porca et al. [10], two types of cavitation can be distinguished: vaporous cavitation and gaseous cavitation. Vaporous cavitation occurs when the pressure drops below the liquid–vapor pressure, and vapor cavities develop in the

liquid. The vaporous cavitation is characterized by the vapor volume fraction α_v, which expresses the fraction of the vapor volume V_v in a given volume of fluid V (vapor + liquid):

$$\alpha_v = \frac{V_v}{V} \tag{1}$$

For low values of α_v ($\alpha_v \approx 0$), tiny vapor bubbles are dispersed throughout the liquid. This regime is referred to as "dispersed cavitation." This type of cavitation occurs over an extended length of the pipe. When the vapor cavities coalesce, they give rise to a single local bubble occupying a large portion of the pipe cross section ($\alpha_v \approx 1$). This regime is known as "column separation," and it is the purpose of the study presented here.

The presence of noncondensable gases (NCGs) dissolved in a liquid can lead to gaseous cavitation. One of the main features of liquids is their ability to absorb a given amount of gas when in contact with the free surface. According to Henry's law [11], at constant temperature, the amount of gas dissolved in a liquid volume is directly proportional to the partial pressure of the gas in equilibrium with the liquid. The gas release occurs when the pressure falls below the saturation pressure, which is a diffusive process that can develop quickly. On the other hand, the absorption process from the gaseous to the dissolved liquid states has to overcome surface tension, and therefore takes longer than the desorption/release process. The presence of gas bubbles in the liquid tends to cushion the impact of the filling fronts [12–14], and it can drastically reduce the wave velocity, thus lowering the pressure rise during fluid hammer, as described in the textbook by Wylie and Streeter [15].

The design of hydraulic systems needs to take into consideration of transient conditions that may occur in pipeline flows. This is normally achieved by using numerical methods. One of them is the method of characteristics (MOC), which has become a standard numerical approach for this problem. All fundamentals can be found in Ref. [15] and in the review by Lohrashi and Attarnejad [16]. In short, the MOC transforms the partial differential equations describing the fluid hammer into ordinary differential equations and integrates them along characteristic lines. This method is based on several assumptions: the velocity is cross-sectional averaged, the pressure is considered uniform across the pipe section, the effects of variations in velocity head are neglected, the variations of the liquid density are disregarded in the momentum equation, the friction factors under steady flow conditions are assumed to hold in unsteady flows, and, finally, the pipe is assumed to be full of liquid at all times. These assumptions cause minor errors in common engineering problems, except for the last two hypotheses. On the one hand, the modeling of unsteady friction was found to reduce the initial flow acceleration [17] and to attenuate the magnitude of pressure spikes during fluid hammer [18–21]. On the other hand, if cavitation or column separation occurs, they must be accounted for with additional conditions to be satisfied, such as in the discrete vapor cavity model, the discrete gas cavity model, and the generalized interface vaporous cavitation model. These models are described and compared against experimental results [22] or, more recently, by using finite volume Godunov-type schemes [23–25].

This work aims at providing insight into the column separation mechanism, which originates after the impact of a liquid front on the closed end of a pipeline initially under vacuum conditions. This is done by integrating the Navier–Stokes momentum equation and defining the appropriate boundary conditions for this particular flow configuration. The integral form of the conservation principles is applied through the pressure waves appearing in the flow in order to close the set of equations. The analysis distinguishes two types of pressure waves: compression and expansion. Compression waves appear right after the fluid hammer pressure rise and travel toward the tank, and then they reflect as expansion waves. The application of the conservation principles to the former leads to Rankine–Hugoniot-like conditions, as well as to similar conditions for the latter. When the expansion wave reaches the closed end, the pressure at this location might drop below the liquid vapor pressure, which would induce the liquid column separation. The present study seeks to understand the physics of the flow during column separation, without resolving the full flowfield. The main advantage of this model is that it allows seeing the influence of process parameters on the column separation quickly as well as how the variables of the problem affect the fluid hammer attenuation process.

II. Flow Configuration

The flow configuration considered in this study is the same as the one described in Ref. [14], in which a pressurized liquid tank is connected to a pipeline with a closed end, referred to as the "test element." The test element features a fast-opening valve (FOV), isolating the pressurized liquid in the tank from the pipe, which is kept under vacuum conditions. This flow configuration is similar to the one in satellite propellant lines before the priming operation, which is initiated by opening the FOV. The facility layout, presented in Fig. 1, is intended to be clamped onto a vertical wall. In the work by Lema et al. [14], it was found through numerical simulations with EcosimPro that gravity has a negligible influence on the fluid hammer in this flow configuration. The vertical layout allows for straight piping between the tank and the closed end, and it avoids the need for singular elements such as elbows upstream of the FOV. Furthermore, a constant pipe inner diameter is used, as in satellite propellant lines, which also helps to simplify data interpretation.

The test vessel is equipped with an ultrasonic transducer to measure the speed of sound in the unconfined liquid. The accelerating liquid flow is generated by opening the FOV with an operating time lower than 40 ms. The test element is a 2-m-long pipeline, made of a T3AL2.5V titanium alloy, with an outer diameter of 0.25 in. (6.35 mm), a wall thickness of 0.016 in. (0.4 mm), and roughness

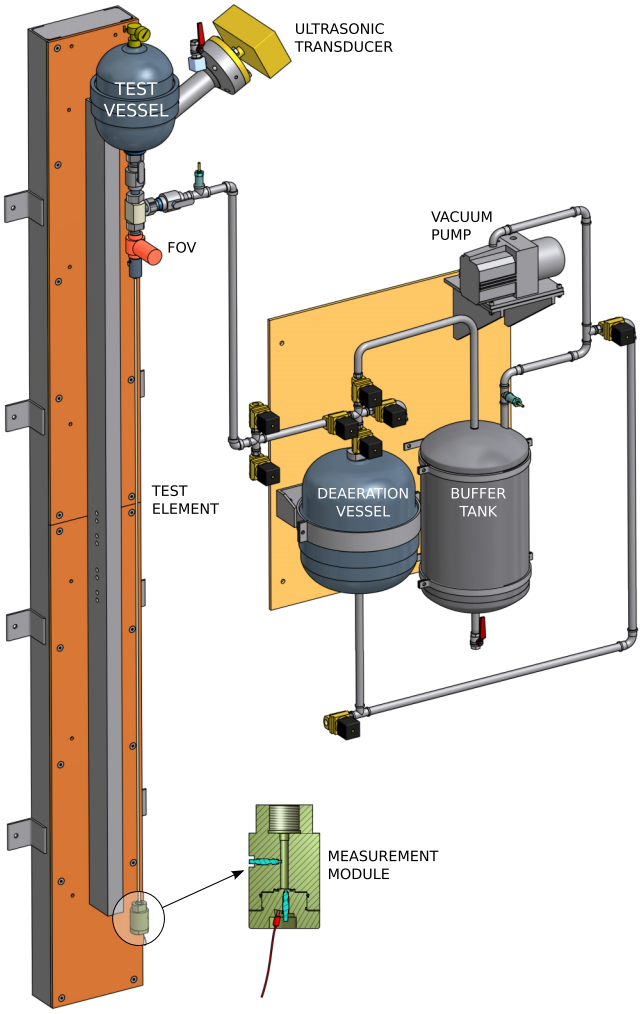

Fig. 1 Experimental facility layout.

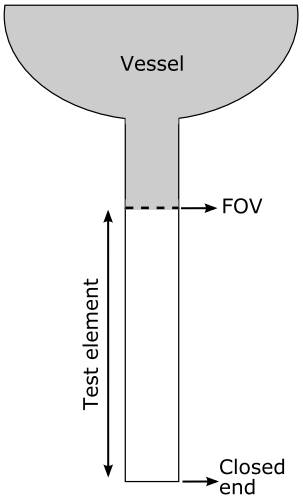

Fig. 2 Experimental configuration.

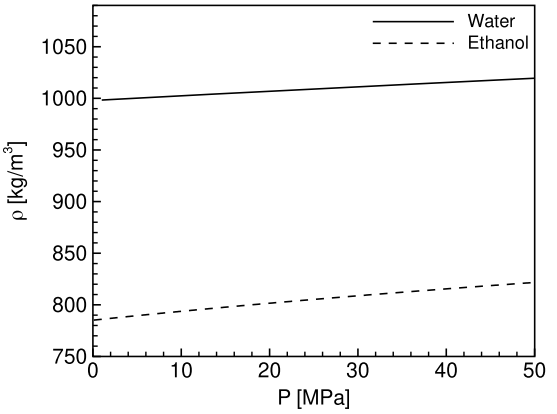

Fig. 3 Densities of water and ethanol as a function of pressure, according to Tait's equation.

of $1.6 \cdot 10^{-6}$ m, resulting in a relative roughness of $\epsilon/D = 2.8 \cdot 10^{-4}$. The total pipe length between the tank and the measurement module is $L = 2.415$ m, which is obtained by adding the test element length (2 m) to the distance between the FOV and the tank (0.415 m).

The test procedure starts by filling the tank with the working liquid to be later pressurized using compressed nitrogen at 2 MPa. The facility is ready for a test when the propellant line is vacuum pumped (1 and 10 kPa are the working values considered in this study), the FOV is closed, and the pipe length between the tank and the FOV is filled with the pressurized working liquid, as sketched in Fig. 2. The test starts by triggering the FOV, which is fully opened before the liquid front reaches the closed end of the pipe.

The facility is designed to run with nonreactive fluids, such as water and ethanol, using nitrogen as the driving pressure NCG. It was found in Ref. [14] that the saturation level of the working fluid with the NCG plays a significant role in the fluid hammer occurrence. In normal conditions, the driving pressure gas gets dissolved in the liquid through a diffusive process, and the saturation level is defined by the pressure applied to the NCG and the storage temperature. The test liquid is fully deaerated using the facility vacuum system to avoid the influence of the dissolved NCG. The test vessel features an elastic membrane to prevent the absorption of the NCG during the liquid pressurization.

III. Liquid Density as a Function of Pressure

The fluid hammer phenomenon is characterized by an energy conversion, in which the kinetic energy of a flow brought to rest transforms into elastic energy. Under these conditions, the working fluid (usually a liquid) cannot be assumed incompressible because its elastic behavior is at the origin of the fluid hammer phenomenon. That is why, even though density variations in liquids are known to be small, they need to be taken into account when modeling the fluid hammer and subsequent column separation by treating the liquid density as a function of pressure. It is worth mentioning that density is also affected by temperature, but its effect has been found to be small [26]. Furthermore, only completely deaerated liquids are considered in this study. Therefore, the density of the liquid will not change due to the growth of NCG bubbles.

In this work, Tait's equation is used. It is a simple relationship between pressure and volume for water [27] that allows obtaining the water density as a function of pressure and two empirical functions, B and C. Equation (2) shows the integrated form of Tait's equation in terms of density:

$$\frac{1}{\rho} = \frac{1}{\rho_0} - \frac{C}{\rho_0} \cdot \log_{10} \frac{B + P}{B + P_0} \tag{2}$$

In this equation, ρ is the density at a given pressure P; and ρ_0 refers to the density at a reference pressure P_0, which is equal to 10^5 Pa here. The empirical coefficient C is independent of temperature and pressure; its value is $C = 0.315$, whereas B is temperature dependent and can be computed as

$$B = 2996 + 7.5554(T - 25) - 0.17814(T - 25)^2 + 608 \cdot 10^{-6}(T - 25)^3 \tag{3}$$

In this equation, B is expressed in bars and T in degrees Celsius. Assuming a constant temperature of 25°C, B takes the value of $B = 2996$ bar. That is the lowest temperature value allowed by this equation and the one assumed in this study. Tait's equation has been satisfactorily applied to compute the density as a function of pressure for other liquids: for example, Tanaka et al. [28] applied this equation to calculate the density of ethanol with an error below 0.2%. They used the constant values of $C = 0.2065$ and $B = 778$ bar with $T = 25$°C. Figure 3 illustrates the evolution of the density of water and ethanol when the pressure increases up to 50 MPa. The slope of the curves corresponds to $1/c^2$, with c as the speed of sound.

IV. Liquid Column Separation Mechanism

Column separation mainly occurs when the pressure in the pipeline drops below the liquid vapor pressure at specific locations, such as the closed end of the present experimental configuration, and is observed with flow visualization in Refs. [6,29]. The present analysis seeks to understand the physics of the column separation occurrence right after the first fluid hammer pressure peak, based on the resolution of the momentum equation.

Just when opening the FOV, the present experimental setup and conditions are similar to the ones found when using one-dimensional expansion tubes to study the phase transition in metastable liquids. For example, Saurel et al. [30] and Simões-Moreira and Shepher [31] used a pressurized liquid that was confined in a pipe between a blind end and a membrane-type FOV. When the FOV opens, the liquid discharges through a short pipe toward a reservoir containing a rarefied gas. Those studies focused on what happens upstream of the FOV, whereas we focus here on what happens downstream. However, the description of the initial instants, such as in the work by Saurel et al. [30], is valid for our case. Following that description, as soon as the membrane between the liquid and the vacuum chamber breaks, a rarefaction wave propagates upstream through the liquid column, lowering its pressure, and thus producing a superheated liquid. Then, a subsonic phase transition front propagates through the superheated liquid from the FOV position, producing at its tail a high-velocity liquid–vapor mixture in thermodynamic equilibrium that moves downstream through the gas, for which the pressure is increased by a compression wave generated when opening the FOV. Things start to differ between the conditions in the two experimental setups when the rarefaction wave moving upstream reaches the end of the tube. In the present case, at that point, the wave reaches the tank with pressurized liquid, where it is reflected as a compression wave

that transmits the tank pressure information back along the tube. As the compression wave passes through the medium, it brings the liquid back to a non-superheated state. When the wave reaches the transition front, that front begins to move downstream, driven by the compressed liquid.

After the process just described, the liquid front travels through the tube, as shown in Fig. 4(a), until it reaches its closed end, where it is brought to rest. The fluid hammer that takes place sets a new flow condition (i.e., flow at rest) and pressure rise, which is transmitted through the liquid column all the way back to the tank in the form of a compression wave (Fig. 4b). It has to be pointed out here that the fluid in the column that has not been yet reached by this compression wave continues flowing toward the bottom end of the tube, still compressing the fluid underneath. Once the compression wave travels all the way back to the tank, the whole liquid column is at rest. The tank contains an almost infinite liquid mass as compared to that in the pipe. Therefore, the pressure in the tank is not significantly altered, and the compression wave gets reflected as an expansion wave (Fig. 4c) that transmits the tank pressure information along the pipe, as described in Ref. [32].

The expansion wave divides the liquid column into two regions: the fluid upstream is at rest, whereas the fluid downstream moves toward the tank. When the expansion wave reaches the lower end, the entire liquid column moves toward the tank. Under these circumstances, the pressure of the liquid at the bottom end drops and may reach values below the vapor pressure, resulting in the formation of a multiphase bubble (mixture of liquid, vapor, and the residual NCG initially left in the test element after vacuum pumping) and inducing the liquid column separation (Fig. 4d).

The maximum velocity that the fluid reaches during the entire process corresponds to a Mach number of the order of 0.1. This fact was confirmed in previous works (i.e., Porca et al. [10] and Pinho et al. [13]). Consequently, it is assumed that all compressibility phenomena take place exclusively in the compression and expansion waves, but not in the rest of the fluid column.

In the review by Bergant et al. [9], the tensile stress of the liquid is described as a metastable condition for the liquid; if the liquid undergoes a transient event, it is governed by nonequilibrium thermodynamics. This means that, in spite of the vapor formation in the growing multiphase bubble that leads to the column separation, the pressure may still be below the vapor pressure of the liquid. Any residual gas in the line or evolving from the liquid will be found in the bubble together with the vapor. According to Dalton's law, the new pressure in the multiphase bubble will be the sum of the partial pressures of each component, increasing the final pressure; but, in the present analysis, the pressure in the multiphase bubble will be assumed to be equal to the vapor pressure.

Published experimental evidence obtained with high-speed imaging by Lema et al. [6] shows that the liquid front approaching the end of the tube (as in Fig. 4a) is not uniform and appears as a foamy

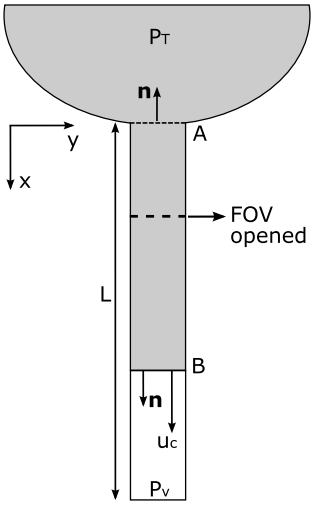

a) Liquid front moving down

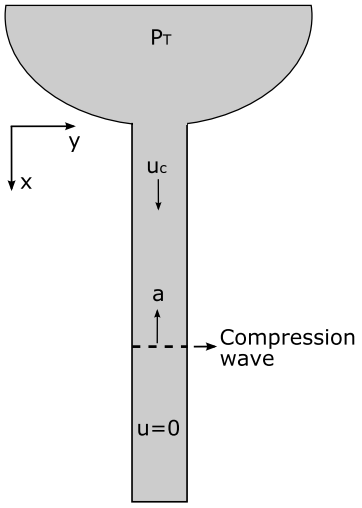

b) Compression wave moving up

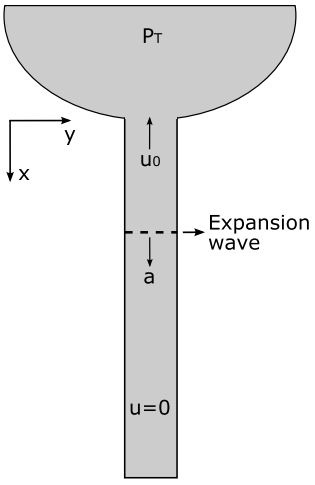

c) Expansion wave moving down

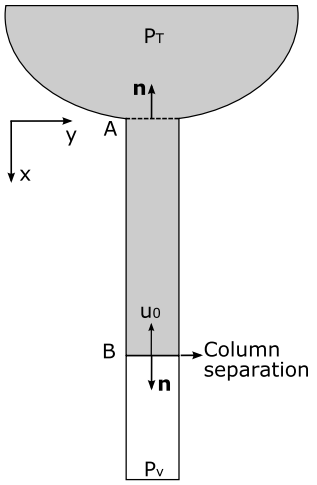

d) Liquid column separation

Fig. 4 Sequence of liquid column dynamics.

mixture of liquid and gas extending over a considerable pipe length of at least 25 pipe diameters. It is due to the occurrence of cavitation at the front, plus the effects of the finite opening time of the FOV. These complex effects do not admit an obvious simplification, except to assume that the liquid front behaves as if it were uniform, which means that the interface is perpendicular to the pipeline and without any mixing between the gas and the liquid phases.

After assuming a uniform liquid front, the motion of the liquid column toward the tank can be described by solving the integral form of the Navier–Stokes momentum equation [Eq. (4)]. Using the control volume shown in Fig. 4d, it can be formulated as

$$\frac{d}{dt}\int_{V_0}\rho\boldsymbol{u}\,\mathrm{d}V+\int_{S_0}\rho\boldsymbol{u}(\boldsymbol{u}-\boldsymbol{u_c})\cdot\boldsymbol{n}\,\mathrm{d}s=\int_{S_0}(-PI+\tau)\cdot\boldsymbol{n}\,\mathrm{d}s+\int_{V_0}\rho\boldsymbol{f_m}\,\mathrm{d}V \tag{4}$$

where V_0 represents the liquid volume in the pipeline, S_0 corresponds to the pipe inlet and outlet cross sections, and $\boldsymbol{u_c}$ is the velocity of the moving control surface. Here, the control volume moves with the liquid column inside the pipe; thus, the bottom control surface (control surface B in Fig. 4) has the same velocity as the liquid column moving toward the tank: $\boldsymbol{u_c}=\boldsymbol{u_0}$. In the resolution of the momentum equation, the following assumptions are made:

1) The pressure at control surface B is assumed to be the vapor pressure, $P_B=P_v$ (the metastable equilibrium is ignored, and there is no gas desorption).

2) Control surface A is at the tank outlet, where the pressure is constant and equal to $P_A=P_T$.

3) The body force due to gravity is assumed to be negligible (the hydrostatic forces are negligible as compared to the dynamic forces).

4) Except when passing through the pressure waves, the liquid in the entire column can be assumed to be incompressible.

5) Friction is treated as steady by means of the Darcy–Weisbach friction factor λ.

This last assumption is made in many transient flow calculations and is commonly adopted in the MOC, as described by Lohrasbi and Attarnejad [16]. Therefore, the wall shear stress in Eq. (4) is considered to be steady; according to the Darcy–Weisbach equation, the friction factor is related to the wall shear stress as follows:

$$\tau_w=-\frac{\rho\lambda U|U|}{8} \tag{5}$$

Therefore, each term of Eq. (4) is solved separately as follows:

$$\frac{d}{dt}\int_{V_0}\rho\boldsymbol{u}\,\mathrm{d}V=\rho A(\ddot{x}x+\dot{x}^2)$$

$$\int_{S_0}\rho\boldsymbol{u}(\boldsymbol{u}-\boldsymbol{u_c})\cdot\boldsymbol{n}\,\mathrm{d}s=-\rho A\dot{x}^2$$

$$\int_{S_0}(-PI+\tau)\cdot\boldsymbol{n}\,\mathrm{d}s=(P_T-P_v)A-\frac{\rho\lambda A}{2D}\dot{x}^2x$$

$$\int_{V_0}\rho\boldsymbol{f_m}\,\mathrm{d}V=\boldsymbol{0}$$

Replacing each term in Eq. (4) leads to

$$\ddot{x}x+\frac{\lambda}{2D}\dot{x}^2x=\frac{P_T-P_v}{\rho} \tag{6}$$

which is a second-order ordinary differential equation. An analytical solution to this equation can be found [17] but, for the sake of simplicity, Eq. (6) is solved when friction is neglected in order to check the role of the main variables of flow on the column separation phenomenon. If friction is neglected (that is, if $\lambda=0$), Eq. (6) becomes

$$\ddot{x}x=\frac{P_T-P_v}{\rho} \tag{7}$$

To solve this equation, two changes of variable are needed to obtain a linear first-order differential equation in the form $dy/dx=f(x)$. The boundary condition at $x=L$ (tube length) is $\dot{x}=u_0$, where u_0 is the velocity of the liquid column moving toward the tank downstream of the expansion wave.

The solution is then

$$u=\sqrt{u_0^2+\frac{2(P_T-P_v)}{\rho}(\ell_n x-\ell_n L)} \tag{8}$$

V. Expansion and Compression Waves' Generation

The only unknown in Eq. (8) is the liquid velocity u_0. This velocity is reached by the liquid column almost instantly when the liquid converts elastic energy into kinetic energy through the expansion wave. The value of u_0 can be determined by applying the model generally proposed for normal shock waves in one-dimensional flow, as in Ref. [33], in which the Rankine–Hugoniot conditions are enforced across the discontinuities generated in the flow. In the case of solids and liquids, and according to the description in Ref. [34], the conservation of mass and momentum are sufficient to determine the initial velocity u_0. This method can be applied to both compression and expansion waves. Therefore, taking a slice of fluid moving with the wave as a control volume, Eqs. (9) and (10) define the conservation of mass and momentum:

$$\rho_f(u_f-u_c)=\rho_b(u_b-u_c) \tag{9}$$

$$\rho_f(u_f-u_c)^2+P_f=\rho_b(u_b-u_c)^2+P_b \tag{10}$$

Within the range in which the values of the variables vary in the present study, the maximum variation of density induced by temperature is 0.4%, whereas the variation produced by pressure is three orders of magnitude higher. This was corroborated, both numerically and experimentally, in previous works [2,14,26]. For this reason, density variations produced by temperature changes are neglected here; just those due to pressure variations are taken into account. That means that the energy conservation equation is not needed because it would be the case to close the Rankine–Hugoniot conditions, which agrees with the approaches used in water hammer analysis [15,32] and shock waves in liquids and solids [34]. Furthermore, the equations are valid for both compression waves and expansion waves. In the latter case, the wave is continuous, and its thickness increases with time along its trajectory. Thus, it must be ensured that the thickness of the wave is small enough to be negligible at all times. In the present flow configuration, it is the case, as evidenced by the fact that the pressure drop time of the water hammer is practically identical to its rise time. On the other hand, the diameter-to-pipe wall thickness ratio, D/e, is equal to 14; and the Young modulus of elasticity of the titanium alloy is 10^{11} Pa. For these values, a water hammer with a pressure jump of 200 bar generates a cross-sectional area variation per unit area (dA/A) of about 10^{-4}, which makes it possible to neglect this variation. Therefore, the effects induced by the fluid–structure interaction on the propagation of pressure waves can be ignored, and the waves are considered to have a speed close to the speed of sound.

In Eqs. (9) and (10), subscripts "b" and "f" refer to the fluid behind and in front of the shock or expansion wave, as sketched in Fig. 4. Figure 5 shows the compression (Fig. 5a) and expansion (Fig. 5b) waves (thick dashed line) traveling along the pipe, with the wave velocity a. The control volume is a thin slice of fluid that moves with the wave in both cases, together with an auxiliary reference system (x', y', z') parallel at all times to the reference system of Fig. 4. The fluid behind the expansion wave is moving upward toward the tank, with $P_b=P_T$ (where P_T is the tank pressure) and a relative velocity of $u_b=u_0+a$. Ahead of the expansion wave, the fluid is at rest; so, the relative velocity is $u_f=a$, and the pressure is equal to the fluid

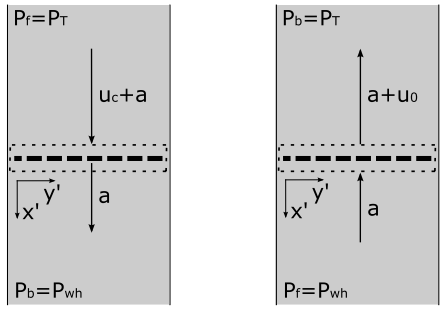

Fig. 5 Control volume used to solve the a) compression wave and b) the expansion wave traveling in the liquid column.

hammer pressure increase: $P_f = P_{\text{wh}}$. Solving Eqs. (9) and (10) in the control volume defined in Fig. 5, the following system of equations is obtained:

$$\rho_f a = \rho_b(a + u_0) \tag{11}$$

$$\rho_f a^2 + P_{\text{wh}} = \rho_b(a + u_0)^2 + P_T \tag{12}$$

Similarly, the equations corresponding to the compression wave can be obtained. The only unknowns in Eqs. (11) and (12) are the velocity behind the wave, $u_b = u_0$, and the wave speed a because the local density in the flow regions behind and in front the wave can be obtained using Tait's equation [Eq. (2)]. The solution to the system of equations [Eqs. (11–12)] is

$$u_0 = a\left(\frac{\rho_f}{\rho_b} - 1\right) \tag{13}$$

$$a = \sqrt{\frac{P_{\text{wh}} - P_T}{\rho_f[(\rho_f/\rho_b) - 1]}} \tag{14}$$

Therefore, Eqs. (13) and (14) allow us to conclude that the velocity of the liquid column moving toward the tank during column separation and the wave speed are defined by the density change across the expansion wave, which is in turn given by the tank pressure P_T and the pressure rise induced by the fluid hammer P_{wh}. The velocity of the liquid column given by Eq. (8) also depends on the tank pressure and the pressure in the multiphase bubble, which is assumed here to be equal to the vapor pressure P_v, but which can be different due to the metastable equilibrium or the gas desorption.

The value of P_{wh} in Eq. (14) can be computed or measured for a given configuration defined by the pipeline geometry, the tank pressure, and the vacuum conditions in the test element. Once this value of P_{wh} is available, the model can provide useful engineering guidance on the design, development, and analysis of relevant applications where liquid column separation takes place as a consequence of fluid hammer occurrence.

VI. Results and Validation with Experimental Data

To validate the model proposed in this study, the values of the fluid velocity behind the wave are obtained using the data published by Lema et al. in Ref. [14] for deaerated water and deaerated ethanol at $T = 293$ K, where the test element is made of titanium tubing used for aerospace applications, as described in Sec. II.

First of all, Eqs. (13) and (14) are solved to obtain the velocity u_0. Table 1 shows the solutions across the expansion wave obtained for deaerated water under the indicated experimental conditions. Two tank pressures are used: $P_T = 1$ MPa and $P_T = 2$ MPa, with two initial vacuum conditions in the test element of $P_p = 1$ and 10 kPa. The pressure P_p is not used to solve Eqs. (13) and (14) but has an influence on the P_{wh} value, which is measured experimentally.

Table 1 Solution to the equations of state for the expansion wave computed for deaerated water for the two first multiphase bubbles

	$P_b = P_T = 2$ MPa, $\rho_b = 998.8$ kg/m^3				$P_b = P_T = 2$ MPa, $\rho_b = 998.4$ kg/m^3	
	$P_b = 1$ kPa		$P_b = 10$ kPa		$P_b = 1$ kPa	
Separation bubble	First	Second	First	Second	First	Second
$P_f = P_{\text{wh}}$ [MPa]	21.0	11.5	18.9	9.8	16.6	9.2
ρ_f [kg/m^3] at P_{wh}	1007.2	1003.1	1006.4	1002.3	1005.4	1002.1
a [m/s]	1491.6	1482.7	1487.2	1479.5	1432.2	1487.9
$u_b = u_0$ [m/s]	12.64	6.38	11.29	5.26	10.43	5.48

Table 2 Solution to the equations of state for the expansion wave computed for deaerated ethanol for the two first multiphase bubbles

	$P_b = P_T = 2$ MPa, $\rho_b = 786.9$ kg/m^3			
	$P_b = 1$ kPa		$P_b = 10$ kPa	
Separation bubble	First	Second	First	Second
$P_f = P_{\text{wh}}$ [MPa]	17.3	10.6	16.7	10.2
ρ_f [kg/m^3] at P_{wh}	799.3	794.0	798.9	793.7
a [m/s]	1091.8	1080.4	1089.3	1077.5
$u_b = u_0$ [m/s]	17.48	10.02	16.89	9.58

Table 2 shows the solutions across the expansion wave obtained for deaerated ethanol at $T = 293$ K, where the tank pressure is always $P_T = 2$ MPa, with two initial vacuum conditions in the test element: $P_p = 1$ and 10 kPa.

Once the velocity of the liquid column moving toward the tank is known (last rows of Tables 1 and 2), Eq. (6) can be solved by numerical integration using the vapor pressure of both liquids at 293 K ($P_v = 2.3$ kPa for water and $P_v = 5.95$ kPa for ethanol) and satisfying the condition that at the closed end ($L = 2.4156$ m), the liquid front velocity is $-u_0$ (negative value because the liquid is moving toward the tank). The Darcy–Weisbach friction factor was estimated to be approximately 0.02 with both liquids. This value corresponds to a Reynolds number of approximately $6 \cdot 10^4$ in the Moody diagram for both water at 20 m/s and ethanol at 14 m/s, which are the highest velocities observed experimentally.

Figure 6 shows the position of the liquid front for both liquids together with the duration of the liquid column separation represented in the x axis. These graphs were obtained with the data measured after the first fluid hammer pressure rise when the initial vacuum pressure in the test element was $P_p = 1$ kPa and the pressure in the tank was $P_T = 2$ MPa.

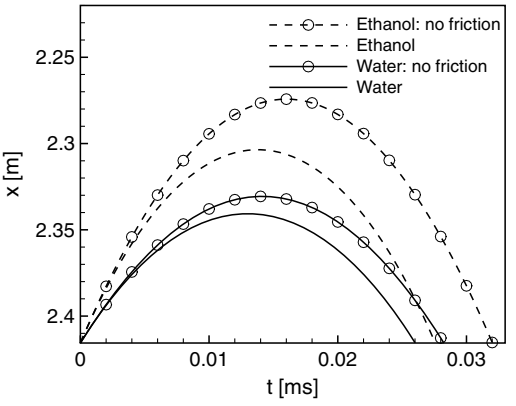

Fig. 6 Numerical solution to Eq. (6) solved with and without friction for both deaerated water and deaerated ethanol.

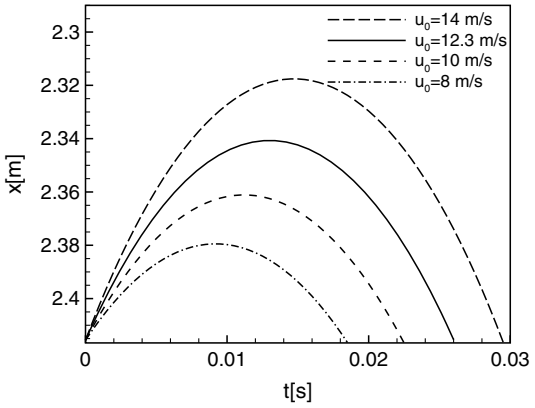

Fig. 7 Comparison of the liquid column separations for different initial velocities with deaerated water.

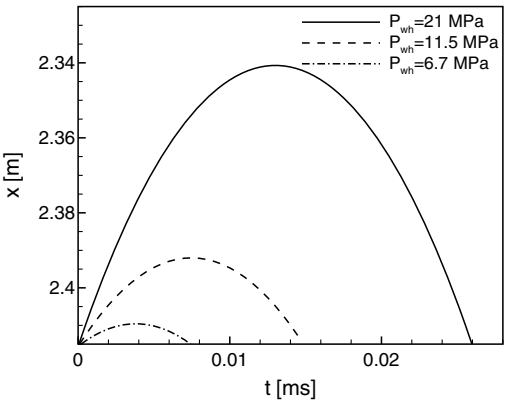

Fig. 8 Numerical solution for deaerated water with $P_T = 2$ MPa and different P_{wh} values.

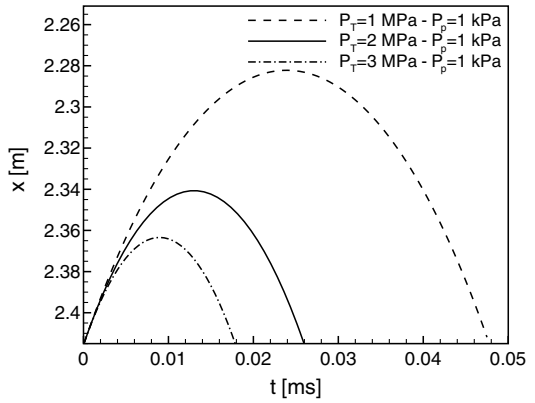

Fig. 9 Numerical solutions for deaerated water for different P_T values.

The multiphase bubble left behind grows and exerts a low pressure that counterbalances the motion of the liquid column. According to Fig. 6, the liquid column stops moving toward the tank after 13 ms for water and 14 ms for ethanol. At this point, the liquid column starts moving again toward the closed end. The second front impact takes place after 26 ms for water and 28 ms for ethanol, which generates another pressure rise; and the whole cycle starts over again. To observe the influence of friction on the column separation phenomenon, the solution of Eq. (6) when $\lambda = 0$ is also plotted in Fig. 6 for both liquids. It is observed that, without the energy dissipation caused by friction, the liquid column travels a larger length in the pipeline, resulting in a longer duration of the liquid column separation. Therefore, friction plays an important role and cannot be dismissed from the analysis.

According to Eq. (8), the phenomenon of liquid column separation is produced by the liquid column moving upward behind the expansion wave. A higher velocity will result in a larger multiphase bubble, as can be seen in Fig. 7, resulting in a longer delay between peaks and a higher velocity when the liquid column reaches again the closed end. The velocity depends mainly on the wave velocity, which grows with the pressure peak value P_{wh} and decreases with the tank pressure P_T, as stated in Eq. (14). Figure 8 shows the numerical solution of Eq. (6) using the three first fluid hammer pressure peaks measured with deaerated water [14]. One can observe that the column separation takes longer with higher-pressure levels. On the other hand, Fig. 9 shows the opposite behavior when the pressure in the tank increases.

If the pressure increase during the fluid hammer is not sufficiently high, the acceleration of the liquid column toward the tank is not sufficient to induce the column separation. Under those circumstances, the period between pressure peaks is obtained with Eq. (15), which represents the time needed for the compression wave to reach the tank and the expansion wave to travel back to the closed end, with both moving at the wave speed in the liquid:

$$t = \frac{2L}{a} \tag{15}$$

To check that the model can predict the liquid column separation behavior, the solution of Eq. (6) is plotted against the pressure evolution measured experimentally by the authors at the closed end. Figure 10 shows the results with deaerated water, where the time window spans over the three first pressure peaks, and the liquid column separation takes place twice: between the first and second peaks and between the second and third peaks. The first liquid column separation has already been plotted in Fig. 6 for water and ethanol by taking friction into consideration. When this result is plotted together with the pressure measurements, adjusting the time reference of the theoretical results to coincide with the first pressure peak, we can observe that the model correctly predicts the time delay between peaks for the first column separation, as evidenced in Figs. 10–12. The error is always lower than 5% in the duration of the first multiphase bubble. The same exercise can be done for the

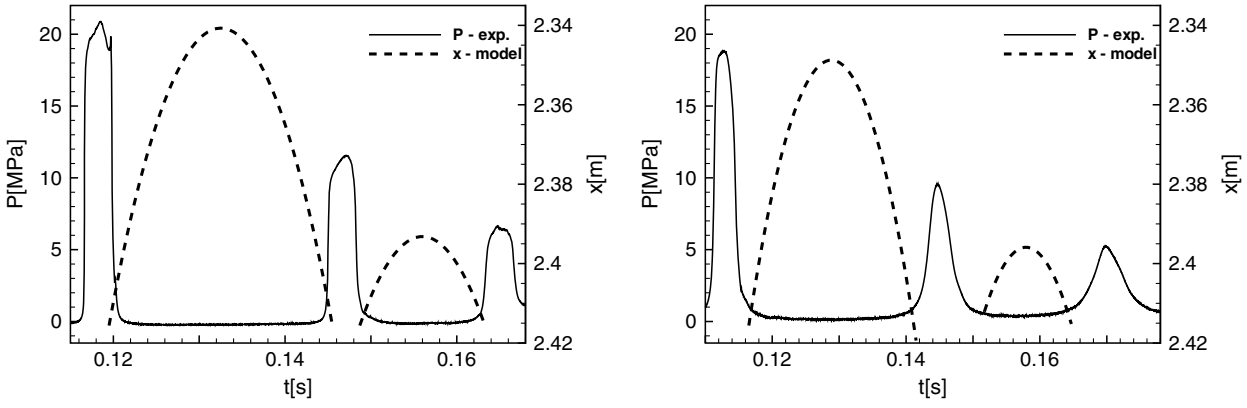

Fig. 10 Theoretical column separation computed for first and second peaks and compared to experimental (exp.) data. Test case for deaerated water: $P_T = 2$ MPa and $P_p = 1$ kPa (left), and $P_p = 10$ kPa (right).

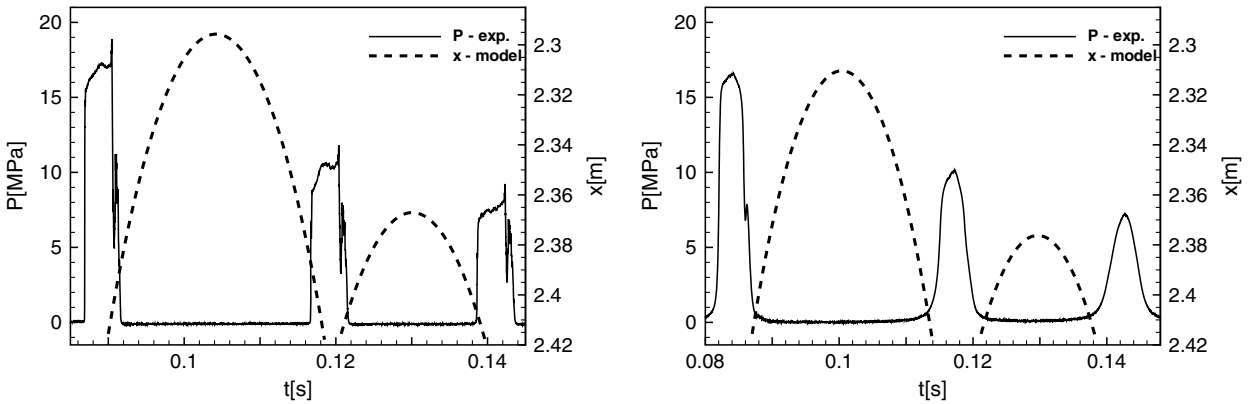

Fig. 11 Theoretical column separation computed for first and second peaks and compared to experimental data. Test case for deaerated ethanol: $P_T = 2$ MPa and $P_p = 1$ kPa (left), and $P_p = 10$ kPa (right).

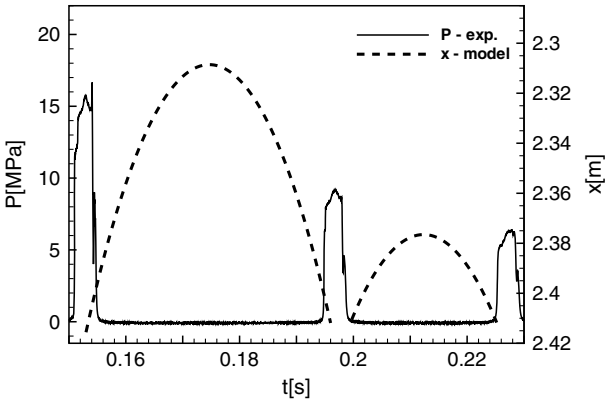

Fig. 12 Theoretical column separation computed for first and second peaks and compared to experimental data. Test case for deaerated water: $P_T = 1$ MPa and $P_p = 1$ kPa.

second liquid column separation, which takes place between the second and third peaks. The result is also plotted in Fig. 10. The time delay predicted theoretically for the second column separation also agrees with the experimental results when $P_p = 1$ kPa, but the error increases to 27% with water and 19% with ethanol when $P_p = 10$ kPa. That is because, in this test condition, the presence of NCGs in the multiphase bubble increases accordingly when Eq. (8) assumes that the pressure in the bubble is always equal to the liquid vapor pressure.

VII. Conclusions

This paper presents a theoretical model to predict the liquid column separation when an accelerated liquid column reaches a closed end of a pipe initially kept under vacuum conditions. This flow configuration is found in propulsion systems used in satellites during priming operation when the pressurized propellant stored in the fuel tank fills the evacuated propellant lines. Under these circumstances, the generated fluid hammer induces a liquid column separation that leaves a multiphase bubble behind. The proposed model is the result of integrating the Navier–Stokes momentum equation for the liquid column and applying the integral form of the conservation principles to the pressure waves traveling along the pipe. First, a compression wave generated at the fluid hammer travels toward the tank where the liquid is stored. Then, a reflected wave travels as an expansion wave back to the bottom end, accelerating behind the liquid column toward the tank and inducing the liquid column separation when the expansion wave reaches the closed end. In any case, the effect of temperature on the compressibility of the liquid is negligible. Therefore, it is not necessary to use the energy conservation equation to complete the set of equations. That also leads to the assumption that both compression and expansion waves behave similarly. The initial velocity of the liquid column moving toward the tank during column separation is defined by the density change across the discontinuity computed with Tait's equation and, mainly, by the wave speed, which is obtained from the values of the tank pressure and that of the previous fluid hammer pressure rise. If the tank pressure is small and the water hammer pressure peak is high, then the multiphase liquid column separation bubble grows larger. Finally, the theoretical results satisfactorily compare against experimental data, and the model is accurate for low values of initial vacuum pressure in the pipeline. The present model is simple enough to quickly unravel the influence of process parameters during priming with no need to compute the total flow.

Acknowledgments

This research was supported by the Xunta de Galicia and the European Regional Development Funds under grant EDC431C-2021/39 and the Spanish Science and Education Ministry through grant RTI2018-101114-B-I00. We wish to acknowledge the support received from the Centro de Investigación de Galicia, funded by Xunta de Galicia and the European Regional Development Fund-Galicia 2014–2020 Program through grant ED431G 2019/01. The present research activity was promoted by the European Space Research and Technology Centre of the European Space Agency through the General Support Technology Programme (GSTP) activity AO/1-6210/09/NL/CP.

References

[1] Gibek, I., and Maisonneuve, Y., "Waterhammer Tests with Real Propellants," *41st AIAA/ASME/SAE/ASEE Joint Propulsion Conference and Exhibit*, AIAA Paper 2005-4081, AIAA, 2005, pp. 1–10. https://doi.org/10.2514/6.2005-4081

[2] Lecourt, R., and Steelant, J., "Experimental Investigation of Waterhammer in Simplified Feed Lines of Satellite Propulsion Systems," *Journal of Propulsion and Power*, Vol. 23, No. 6, 2007, pp. 1214–1224. https://doi.org/10.2514/1.29269

[3] Adamkowski, A., and Lewandowski, M., "Investigation of Hydraulic Transients in a Pipeline with Column Separation," *Journal of Hydraulic Engineering*, Vol. 138, No. 11, 2012, pp. 935–944. https://doi.org/10.1061/(ASCE)HY.1943-7900.0000596

[4] Adamkowski, A., and Lewandowski, M., "Cavitation Characteristics of Shutoff Valves in Numerical Modeling of Transients in Pipelines with Column Separation," *Journal of Hydraulic Engineering*, Vol. 141, No. 2, 2015, Paper 04014077. https://doi.org/10.1061/(ASCE)HY.1943-7900.0000971

[5] Himr, D., "Investigation and Numerical Simulation of a Water Hammer with Column Separation," *Journal of Hydraulic Engineering*, Vol. 141, No. 3, 2015, Paper 04014080. https://doi.org/10.1061/(ASCE)HY.1943-7900.0000967

[6] Lema, M., López Peña, F., Buchlin, J.-M., Rambaud, P., and Steelant, J., "Analysis of Fluid Hammer Occurrence with Phase Change and Column Separation due to Fast Valve Opening by Means of Flow Visualization," *Experimental Thermal and Fluid Science*, Vol. 79,

Dec. 2016, pp. 143–153.
https://doi.org/10.1016/j.expthermflusci.2016.07.008

[7] Ramezani, L., and Karney, B., "Water Column Separation and Cavity Collapse for Pipelines Protected with Air Vacuum Valves: Understanding the Essential Wave Processes," *Journal of Hydraulic Engineering*, Vol. 143, No. 2, 2017, Paper 04016083.
https://doi.org/10.1061/(ASCE)HY.1943-7900.0001235

[8] Malekpour, A., and Karney, B., "Column Separation and Rejoinder During Rapid Pipeline Filling Induced by a Partial Flow Blockage," *Journal of Hydraulic Research*, Vol. 52, No. 5, 2014, pp. 693–704.
https://doi.org/10.1080/00221686.2014.905502

[9] Bergant, A., Simpson, A., and Tijsseling, A., "Water Hammer with Column Separation: A Historical Review," *Journal of Fluids and Structures*, Vol. 22, No. 2, 2006, pp. 135–171.
https://doi.org/10.1016/j.jfluidstructs.2005.08.008

[10] Porca, P., Lema, M., Rambaud, P., and Steelant, J., "Experimental and Numerical Multiphase-Front Fluid Hammer," *Journal of Propulsion and Power*, Vol. 30, No. 2, 2014, pp. 368–376.
https://doi.org/10.2514/1.B34832

[11] Brennen, C. E., *Cavitation and Bubble Dynamics*, Cambridge Univ. Press, Cambridge, MA, 2013, pp. 48–54.
https://doi.org/10.1017/CBO9781107338760

[12] Wang, L., Wang, F., Karney, B., and Malekpour, A., "Numerical Investigation of Rapid Filling in Bypass Pipelines," *Journal of Hydraulic Research*, Vol. 55, No. 5, 2017, pp. 647–656.
https://doi.org/10.1080/00221686.2017.1300193

[13] Pinho, J., Lema, M., Rambaud, P., and Steelant, J., "Multiphase Investigation of Water Hammer Phenomenon Using the Full Cavitation Model," *Journal of Propulsion and Power*, Vol. 30, No. 1, 2014, pp. 105–113.
https://doi.org/10.2514/1.B34833

[14] Lema, M., López Peña, F., Rambaud, P., Buchlin, J.-M., and Steelant, J., "Fluid Hammer with Gas Desorption in a Liquid-Filling Tube: Experiments with Three Different Liquids," *Experiments in Fluids*, Vol. 56, No. 9, 2015, Paper 180.
https://doi.org/10.1007/s00348-015-2043-2

[15] Wylie, E. B., and Streeter, V. L., *Fluid Transients in Systems*, Prentice–Hall, Upper Saddle River, NJ, 1993, pp. 31–63, 139–142.

[16] Lohrasbi, A., and Attarnejad, R., "Water Hammer Analysis by Characteristic Method," *American Journal of Engineering and Applied Sciences*, Vol. 1, No. 4, 2008, pp. 287–294.
https://doi.org/10.3844/ajeassp.2008.287.294

[17] Tijsseling, A. S., Hou, Q., Bozkuş, Z., and Laanearu, J., "Improved One-Dimensional Models for Rapid Emptying and Filling of Pipelines," *Journal of Pressure Vessel Technology*, Vol. 138, No. 3, 2016, Paper 031301.
https://doi.org/10.1115/1.4031508

[18] Bergant, A., Ross Simpson, A., and Vitkovsky, J., "Developments in Unsteady Pipe Flow Friction Modelling," *Journal of Hydraulic Research*, Vol. 39, No. 3, 2001, pp. 249–257.
https://doi.org/10.1080/00221680109499828

[19] Tiselj, I., and Gale, J., "Integration of Unsteady Friction Models in Pipe Flow Simulations," *Journal of Hydraulic Research*, Vol. 46, No. 4, 2008, pp. 526–535.
https://doi.org/10.3826/jhr.2008.3326

[20] Zhou, L., Liu, D., and Karney, B., "Investigation of Hydraulic Transients of Two Entrapped Air Pockets in a Water Pipeline," *Journal of Hydraulic Engineering*, Vol. 139, No. 9, 2013, pp. 949–959.
https://doi.org/10.1061/(ASCE)HY.1943-7900.0000750

[21] Soares, A. K., Martins, N. M. C., and Covas, D. I. C., "Transient Vaporous Cavitation in a Horizontal Copper Pipe," *Journal of Hydraulic Research*, Vol. 55, No. 5, 2017, pp. 731–736.
https://doi.org/10.1080/00221686.2017.1286394

[22] Bergant, A., and Simpson, A. R., "Pipeline Column Separation Flow Regimes," *Journal of Hydraulic Engineering*, Vol. 125, No. 8, 1999, pp. 835–848.
https://doi.org/10.1061/(ASCE)0733-9429(1999)125:8(835)

[23] Zhao, M., and Ghidaoui, M. S., "Godunov-Type Solutions for Water Hammer Flows," *Journal of Hydraulic Engineering*, Vol. 130, No. 4, 2004, pp. 341–348.
https://doi.org/10.1061/(ASCE)0733-9429(2004)130:4(341)

[24] Seck, A., Fuamba, M., and Kahawita, R., "Finite-Volume Solutions to the Water-Hammer Equations in Conservation Form Incorporating Dynamic Friction Using the Godunov Scheme," *Journal of Hydraulic Engineering*, Vol. 143, No. 9, 2017, Paper 04017029.
https://doi.org/10.1061/(ASCE)HY.1943-7900.0001333

[25] Daude, F., Tijsseling, A., and Galon, P., "Numerical Investigations of Water-Hammer with Column-Separation Induced by Vaporous Cavitation Using a One-Dimensional Finite-Volume Approach," *Journal of Fluids and Structures*, Vol. 83, No. 8, 2018, pp. 91–118.
https://doi.org/10.1016/j.jfluidstructs.2018.08.014

[26] López Peña, F., Lema, M., Rambaud, P., Buchlin, J-M., and Steelant, J., "Temperature Measurements in a Multiphase Fluid Hammer," *11th International Conference on Heat Transfer, Fluid Mechanics and Thermodynamics*, HEFAT, Kruger National Park, South Africa, 2015, pp. 417–420, http://hdl.handle.net/2263/55901 [retrieved 20 July 2015].

[27] Li, Y.-H., "Equation of State of Water and Sea Water," *Journal of Geophysical Research*, Vol. 72, No. 10, 1967, pp. 2665–2678.
https://doi.org/10.1029/JZ072i010p02665

[28] Tanaka, Y., Yamamoto, T., Satomi, Y., Kubota, H., and Makita, T., "Specific Volume and Viscosity of Ethanol-Water Mixtures Under High Pressure," *Review of Physical Chemistry of Japan*, Vol. 47, No. 1, 1977, pp. 12–24, http://hdl.handle.net/2433/47042 [retrieved 20 July 1977].

[29] Bombardieri, C., Traudt, T., and Oschwald, M., "Flow Visualization of the Priming Process in Spacecraft Feedlines," *7th European Conference for Aeronautics and Space Sciences*, 2017, pp. 1–10, https://www.eucass.eu/doi/EUCASS2017-227.pdf.
https://doi.org/10.13009/EUCASS2017-227

[30] Saurel, R., Petitpas, F., and Abgrall, R., "Modelling Phase Transition in Metastable Liquids: Application to Cavitating and Flashing Flows," *Journal of Fluid Mechanics*, Vol. 607, June 2008, pp. 313–350, https://www.cambridge.org/core/product/identifier/S0022112008002061/type/journal_article.
https://doi.org/10.1017/S0022112008002061

[31] Simões-Moreira, J. R., and Shepher, J. E., "Evaporation Waves in Superheated Dodecane," *Journal of Fluid Mechanics*, Vol. 382, No. 11, 1999, pp. 63–86.
https://doi.org/10.1017/S0022112098003796

[32] Parmakian, J., *Waterhammer Analysis*, Dover, New York, 1963, pp. 25–29.

[33] Anderson, J. D., *Modern Compressible Flow: With Historical Perspective*, 4th ed., McGraw–Hill, New York, 2021, pp. 195–234.

[34] Graham, R. A., Asay, J. R., and Shahinpoor, M., *High-Pressure Shock Compression of Solids. Chapter Equations of state*, Springer, New York, 1993, pp. 74–113.

K. A. Gonthier
Associate Editor